Errors of Interannual Variability and Trend in Dynamical Downscaling of Reanalysis

Masao Kanamitsu,[1] Kei Yoshimura,[1] Yoo-Bin Yhang,[2] and Song-You Hong[2]

[1]   The interannual variability of dynamically downscaled analysis and its error relative to global coarse resolution analysis is examined in this paper. The regional model error is shown to significantly contaminate the interannual variability of the seasonal mean. The error occupies a significant part of the interannual variability, particularly during the summer season. Accordingly, the leading modes of empirical orthogonal functions (EOFs) of 500 hPa height in the region differ greatly from those of global analysis. In this paper a variant of spectral nudging, the scale selective bias correction (SSBC) method, is refined to further reduce the error within the observational error. Application of this method in dynamical downscaling reduced the error of the interannual variability of analysis fields (namely, height, temperature, and winds), and made the EOFs of seasonal mean at 500 hPa height agree well with those of the global analysis. Application of the SSBC had a modest impact on model-derived fields, such as precipitation and near-surface air temperature. The improvements in these fields are not as dramatic as those in the analysis fields, but the increased simulation skill is evident. A possible cause of the error in the interannual variability is discussed. No apparent systematic reduction in high-frequency variability is found, and the error in interannual variability is more likely due to excitation of the stationary computational mode by the lateral boundary forcing and ill-posed lateral boundary condition.

1.   Introduction

[2]   Dynamical downscaling has been used extensively for small-scale regional analyses, forecasts, and simulations for the past two decades or more. In recent years focus has shifted toward dynamical downscaling of climate time scale and global change simulations, owing to the public demand for prediction and projection of the impact of global changes on local communities and society. In fact, downscaling has been a major topic in the Intergovernmental Panel on Climate Change (IPCC) assessment from its inception (Climate Change 1995; available at http://www.ipcc.ch/pdf/climate-changes-1995/ipcc-2nd-assessment/2nd-assessment-en.pdf) and the demand continues to grow [*IPCC*, 2007].

[3]   Unfortunately, no numerical models are perfect, and all simulations suffer from systematic and transient errors of some magnitude. Regional models are no exception. Regional model error can appear in two ways. One is characterized by the model physics error, for which even perfect atmospheric forcing cannot simulate observed fields, namely, precipitation, cloudiness, and radiation fluxes. The other is error due to the regional model dynamics: namely, resolution, finite-difference approximations, lateral boundary conditions, and basic assumptions on dynamics (e.g., hydrostatic vs. nonhydrostatic). Among these, the lateral boundary condition is notorious because of its mathematical ill posedness [*Davies*, 1976, 1983].

[4]   The spatial and temporal characteristics of regional model error are also of great importance to regional climate studies. In this paper, we examine the effect of regional model atmospheric error on a long climate time scale, namely, the interannual variability. By nature, this implies a synoptic to planetary scale, owing to the dominant role of such scales in interannual variability [*Blackmon*, 1976] of monthly and seasonal means.

[5]   A part of the regional model "error" can be estimated if we perform a downscaling of reanalysis. In this case the approximate truth is known for analysis fields whose scales are greater than a predetermined value for which the analysis error is considered to be within the observational error. When estimated from the spatial density of the available observations, this scale is of the order of 500 to 1000 km in most operationally produced global objective analyses. Thus it is possible to extract the time-varying "error" for scales greater than this synoptic scale when performing a downscaling of global analysis.

[6]   In this paper we demonstrate that the error part of the climate time scale atmospheric variability is very large and

[1]Scripps Institution of Oceanography, University of California, San Diego, La Jolla, California, USA.
[2]Department of Atmospheric Sciences and Global Environment Laboratory, Yonsei University, Seoul, Korea.
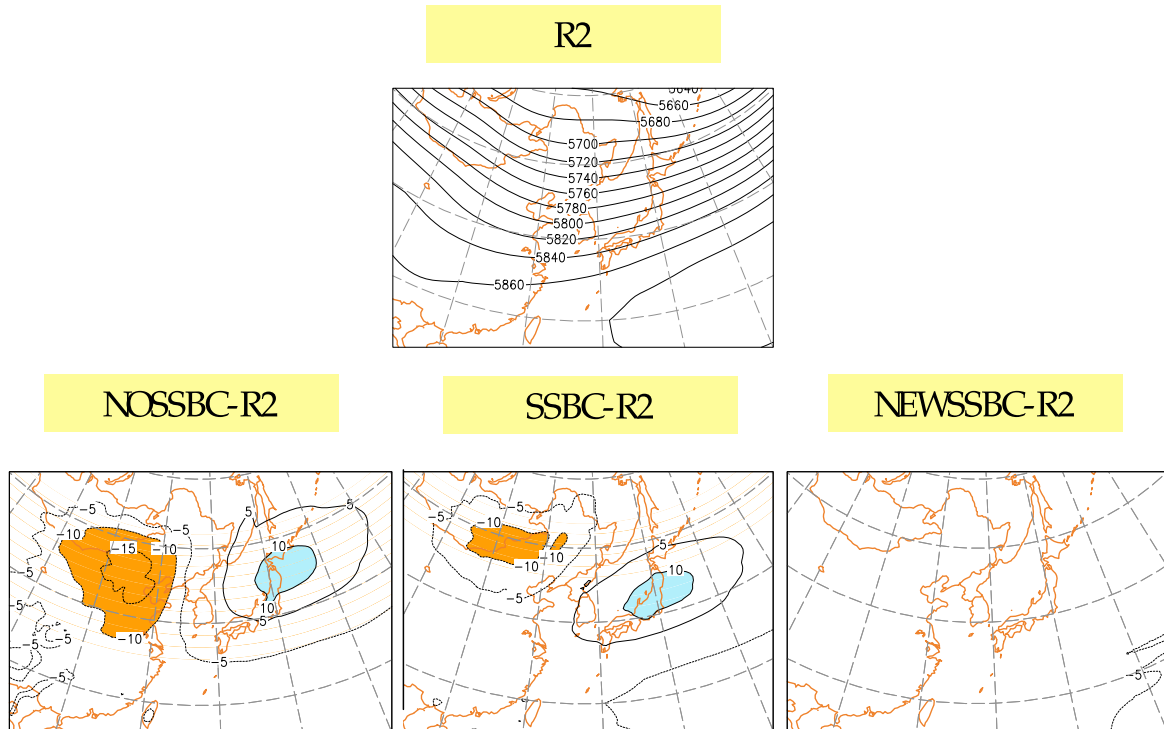
Figure 1. The 1979–2003 summer (June-July-August) climatology at a 500 hPa geopotential height. R-2: National Centers for Environmental Prediction/Department of Energy (NCEP/DOE) reanalysis. Errors of runs without the scale selective bias correction (SSBC; NOSSBC-R2), with the original SSBC (SSBC-R2), and with the refined SSBC (NEWSSBC-R2) are shown in the second row. Units are meters.

significantly contaminates the interannual variability of the synoptic- and planetary-scale portion of the downscaled field. We also show that the contamination of interannual variability affects the long-term linear trend.

[7] One caution should be exercised regarding the definition of error. On the climate time scale, often "truth" does not exist owing to the chaotic nature of the atmosphere. This is because even the observed state is considered to be just a single realization of possible outcomes. In this situation the difference between model simulation and observation is just one of the possible errors. Therefore, it might more appropriately be called "deviation from observation" rather than error. We should note, however, that since we deal with a large number of realizations in running the model for many years, the deviation from observation may be reasonably well regarded as error in the conventional sense. While aware of this complexity, we use the term error in this paper.

[8] The foregoing issues imply that it is important to introduce some sort of "correction" to prevent the model error from contaminating the downscaled analysis. We present that a variant of the spectral nudging method, the scale selective bias correction (SSBC) proposed by *Kanamaru and Kanamitsu* [2006], hereafter referred to as KK06, is a powerful method for performing this error correction. It is shown that, with additional improvements of the method, the error can even be reduced to the range of observational error.

[9] We describe the experiment design in section 2. Section 3 discusses the effect of model error on interannual variability. Section 4 examines the interannual variability of derived fields, namely, near-surface temperature and precipitation. The systematic error in day-to-day variability is discussed in section 5. Conclusions are given in section 6.

2. Model and Experimental Setup

2.1. Model

[10] The spectral representation of the regional spectral model (RSM) is a two-dimensional cosine series for perturbations of pressure, divergence, temperature, and mixing ratio and a sine series for vorticity [*Juang and Kanamitsu*, 1994; *Juang et al.*, 1997]. The spectral method is known to be free from numerical discretization error and is superior to low-order finite-difference formulations. This fact is referenced later in the paper. The physical processes in the RSM follow the package of *Hong and Leetmaa* [1999], except for the revised vertical diffusion scheme of *Hong et al.* [2006]. Long- and short-wave radiation interacting with clouds, nonlocal treatment for the planetary boundary layer process, deep and shallow convection, large-scale condensation, gravity wave drag, hydrology model, and vertical

JJA 25-year 850-hPa wind climatology and error (m/s)

R2

NOSSBC-R2   SSBC-R2   NEWSSBC-R2

blue > 1m/s ,   orange < -1m/s
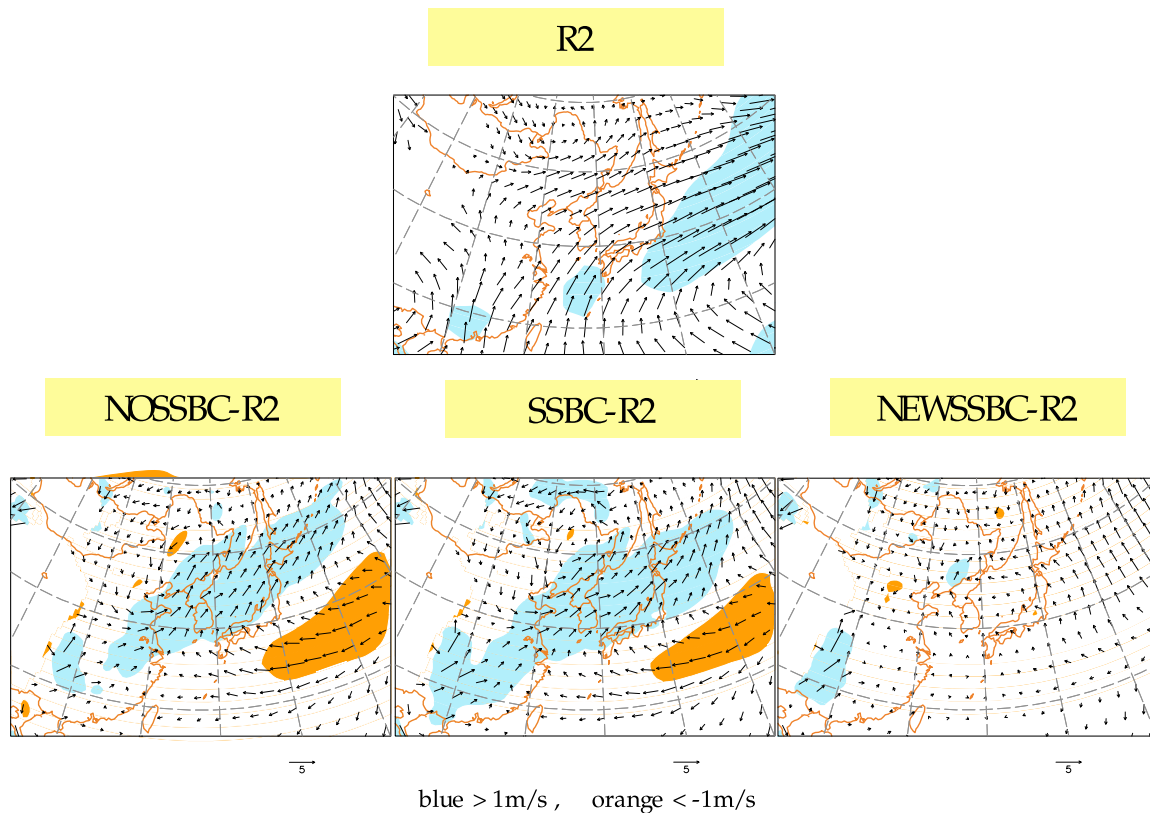
Figure 2. Same as Figure 1 but for 850 hPa winds. Units are meters per second. Blue shading for wind speed overestimation of >5 m/s; brown shading for underestimation of >5 m/s.

and horizontal diffusion are considered. Land surface and soil physics use the two-layer model of *Mahrt and Pan* [1984], which includes soil thermodynamics and hydrology as diffusion processes. Precipitation is produced by both large-scale condensation and convective parameterization schemes. The large-scale precipitation algorithm tests for supersaturation in the predicted specific humidity. Latent heat is released when specific humidity exceeds saturation and the temperatures and humidity are adjusted to bring the humidity to saturation. The scheme does not include a prognostic cloud; however, the evaporation of rain in unsaturated layers below the level of condensation is taken into account.

[11] The two SSBC methods are applied in this study. The original version applies nudging toward external forcing within the domain. Nudging is applied to the tendency of winds for the scale greater than 1000 km equally at all model levels, and the area average temperature and moisture bias are also removed. In the new version the nudging is applied only to the rotational part of the wind field itself (not the tendency), the area average moisture correction is excluded, and the lateral boundary nudging zone width and strength are reduced. These two versions are described in detail in the Appendix, together with some results from comparison experiments.

2.2. Experimental Design

[12] For the study of interannual variability and trend we chose a model domain covering the East Asia Monsoon region centered at 35°N, 127.5°E, from the eastern flank of the Tibetan Plateau in the west to the northwestern Pacific Ocean in the east (Figure 1). This choice of area is somewhat arbitrary but is believed to represent typical midlatitude circulations. Owing to the general nature of the study the results obtained in this paper are applicable to other areas, as seen in KK06 over the continental United States and over South America as shown in the Appendix, but with different magnitudes of impacts. The western boundary cuts across the Tibetan Plateau, but the RSM is relatively insensitive to the placement of the lateral boundary owing to the use of topography smoothing [*Hong and Juang*, 1998]. The model grids consist of 129 (west-east) × 86 (north-south) grid points at approximately 60 km horizontal separation at 60°N and 28 σ layers in the vertical. Simulations were performed for 25 summers (1 June to 31 August) and winters (1 December to the end of February the following year) from 1979 to 2003. Initial conditions and external forcing were obtained from the 6 hourly National Centers for Environmental Prediction/Department of Energy (NCEP/DOE) reanalysis (R-2) data [*Kanamitsu et al.*, 2002]. Note that the integration is not continuous for 25 years but restarts

DJF 25-year 500-hPa height climatology and error (m)
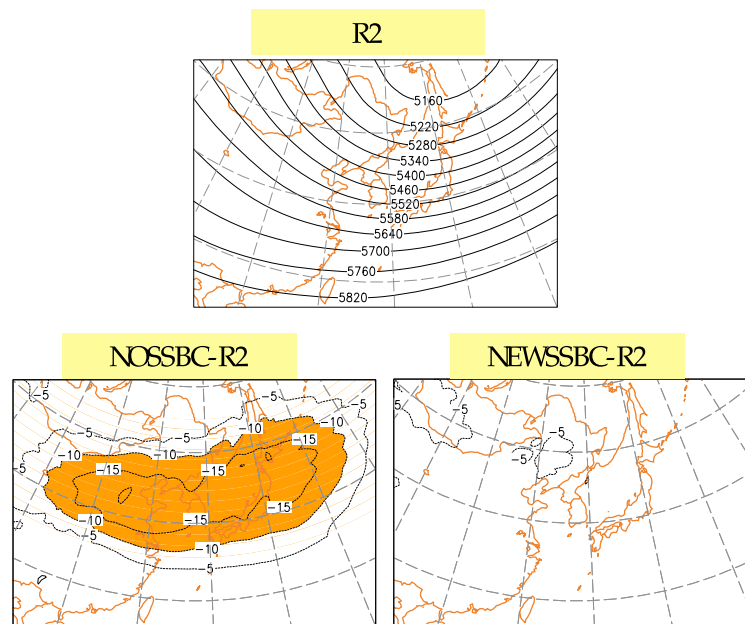
Figure 3. Same as Figure 1 but for 500 hPa height during winter (December-January-February). Units are meters per second. An original SSBC experiment was not performed.

every year for each season 3 months in duration. One of the reasons for this intermittent reinitialization is to save computer resources and time. More importantly, it is intended to exclude large changes in model bottom surface forcing, which might hide the impact of the model error in simulated atmospheric circulation. It should be emphasized that our objective is to examine the impact of simulating synoptic- and planetary-scale atmospheric motion and not to improve the skill of the downscaling. The observed sea surface temperature SST) was updated daily from the optimal interpolation SST weekly data set [*Reynolds and Smith*, 1994]. One may argue that the spin-up is necessary to adjust the soil initial conditions as done in previous studies [e.g., *Gochis et al.*, 2002]. However, preliminary results using the RSM, also described by *Kang and Hong* [2008], showed that spin-up is unnecessary when the RSM is forced by the reanalysis data. This may be because the RSM employs a soil physics package [*Mahrt and Pan*, 1984] and soil and vegetation types similar to those used in the R-2 data assimilation system.

[13] Three experiments are performed without spectral nudging (NOSSBC), with the original SSBC, and with the refined SSBC (NEWSSBC) for summer. For the winter season, only the NOSSBC and NEWSSBC are performed owing to resource limitations.

## 3. Interannual Variability of Geopotential Height and Wind

[14] In this section we analyze the interannual variability of the seasonal mean field simulated by the RSM. We compare the three runs for summer and two runs for winter. Since low-frequency variability tends to have a large spatial scale, synoptic to planetary, these comparisons are equivalent to examining interannual variability and model error of this scale in the regional domain. The small-scale features produced by a high-resolution regional model will also be affected by the simulated synoptic to planetary scale, since the error of this scale affects the location and intensity of the regional scale "system." This is studied in section 4.

3.1. Mean Difference and Interannual Variance

[15] In Figure 1 we show the 1979-2005 R-2 climatology and multiyear mean errors of three model simulations for the summer months. Even for the long-term mean the error in the height field without the SSBC (NOSSBC) is of the order of 10 to 15 m, not negligibly small. This error is only slightly smaller (about 15 m) than the interannual variability shown in Figure 5. The error has a very broad spatial scale, consisting mostly of wave number 1 (in the regional domain) in the east-west direction, with its wavelength of about 2000 km. The error pattern indicates that the climatological trough located over the coast of Russia-China-Korea shifted west and became sharper in summer. Figure 1 also shows that the original SSBC is working to reduce the error moderately, by about 5 m, while the refined SSBC is working well to remove the error, to within 5 m. Similar results are found for 850 hPa winds (Figure 2) and 200 hPa wind speed (not shown), with all this showing that the NOSSBC error is large and the refined SSBC reduces it significantly. Particularly at 850 hPa the error pattern over the Pacific indicates that the northward shift of the subtropical ridge, crucial for summertime simulation over Japan, is nearly eliminated in the NEWSSBC run. This northward shift is a very common model error, found in many simulations [e.g., *Kusunoki et al.*, 2006]. During
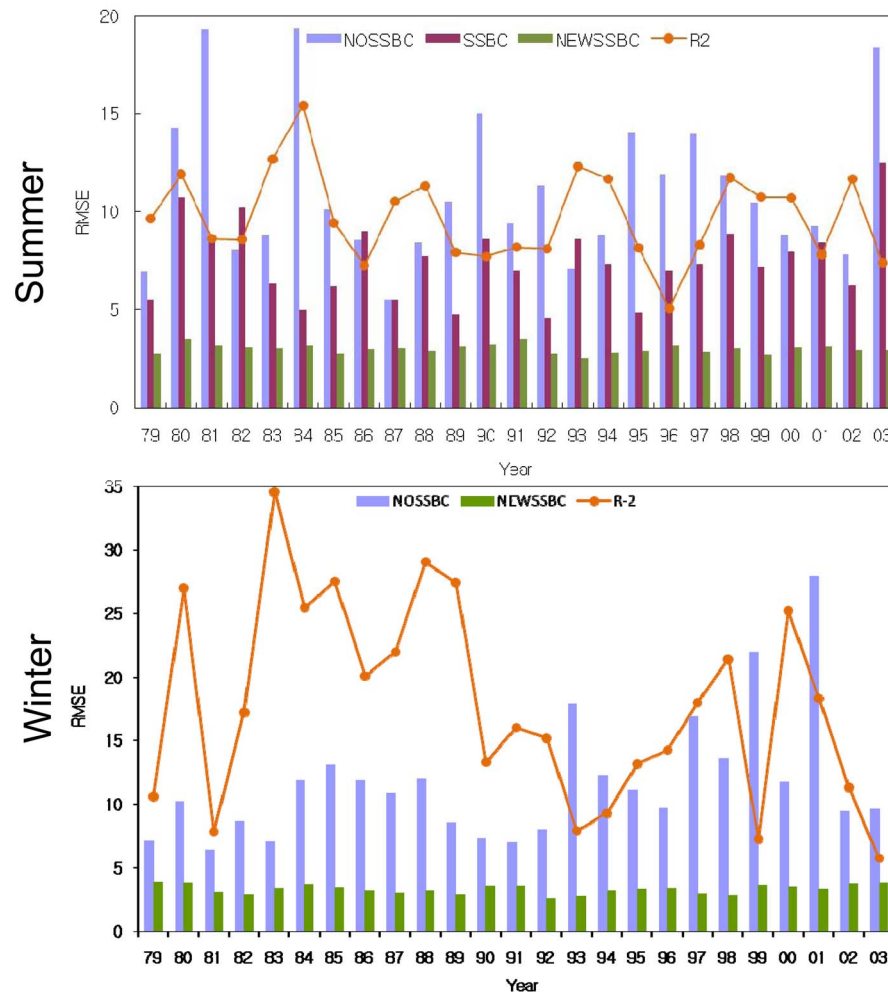
Figure 4. Interannual variability of 500 hPa height root-mean-square error over the domain for summer (top) and winter (bottom). Units are meters. Orange lines indicate interannual variance of height from R-2 observation.

winter the systematic error is larger (Figure 3). The 500 hPa height error for NOSSBC is greater than 15 m and has a much larger east-west extent, indicating a somewhat deeper climatological trough without a shift in location. The NEWSSBC again reduces the error to less than 5 m.

[16] To examine the error evolution by year, Figure 4 displays the year-to-year variability of the root-mean-square (RMS) error of 500 hPa height over the domain for summer (top plot) and winter (bottom plot). The RMS difference between the R-2 analysis and the long-term mean is also plotted as a measure of the interannual variability in Figure 4. It is clearly shown that, without any error correction, the error is large and varies significantly from year to year. The error can become larger than the interannual variability in 11 summers and 4 winters of the 25 years. The error correction is working nicely, as expected, and the new version corrects the error within 2–3 m, with a very small error of interannual variability in both summer and winter.
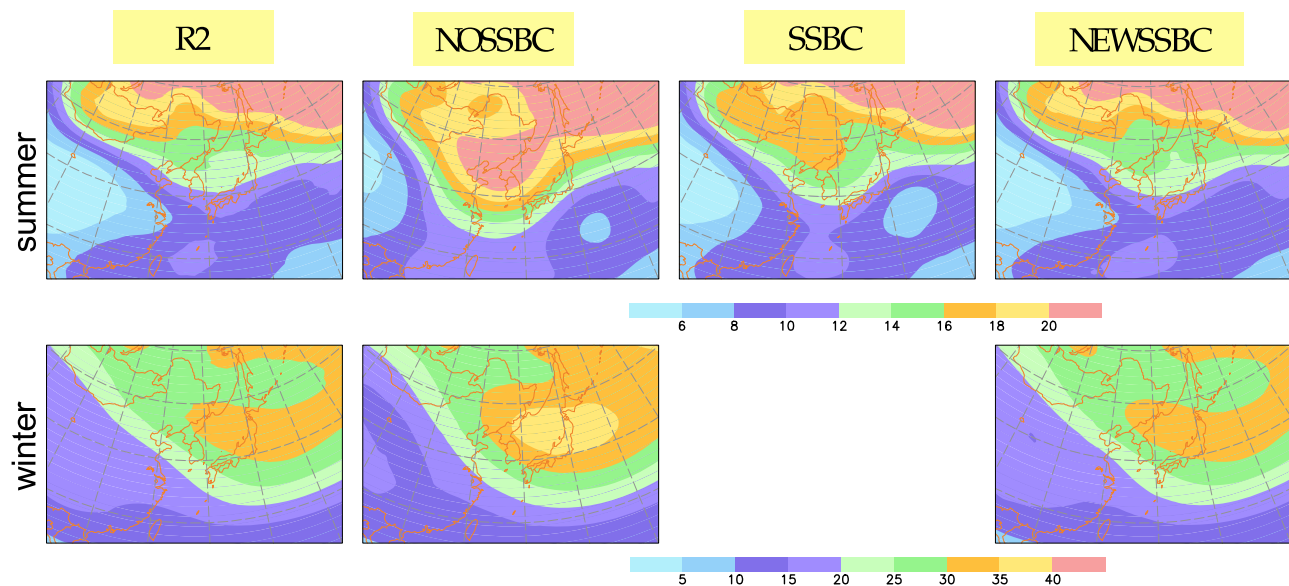
[17] The geographical distribution of interannual variability of 500 hPa height in summer, shown in Figure 5 (first row), clearly demonstrates where the error dominates. The variability is nearly the same between R-2 and the new version of the SSBC, while the run without the SSBC sig-

nificantly increased the interannual variability near the center of the domain, where the variability is more than 30% larger than R-2. During the winter (Figure 5, second row) the interannual variability patterns of R-2 and the NOSSBC are not far apart, although without the SSBC the variability is enhanced by 10%–20% in the middle of the region.
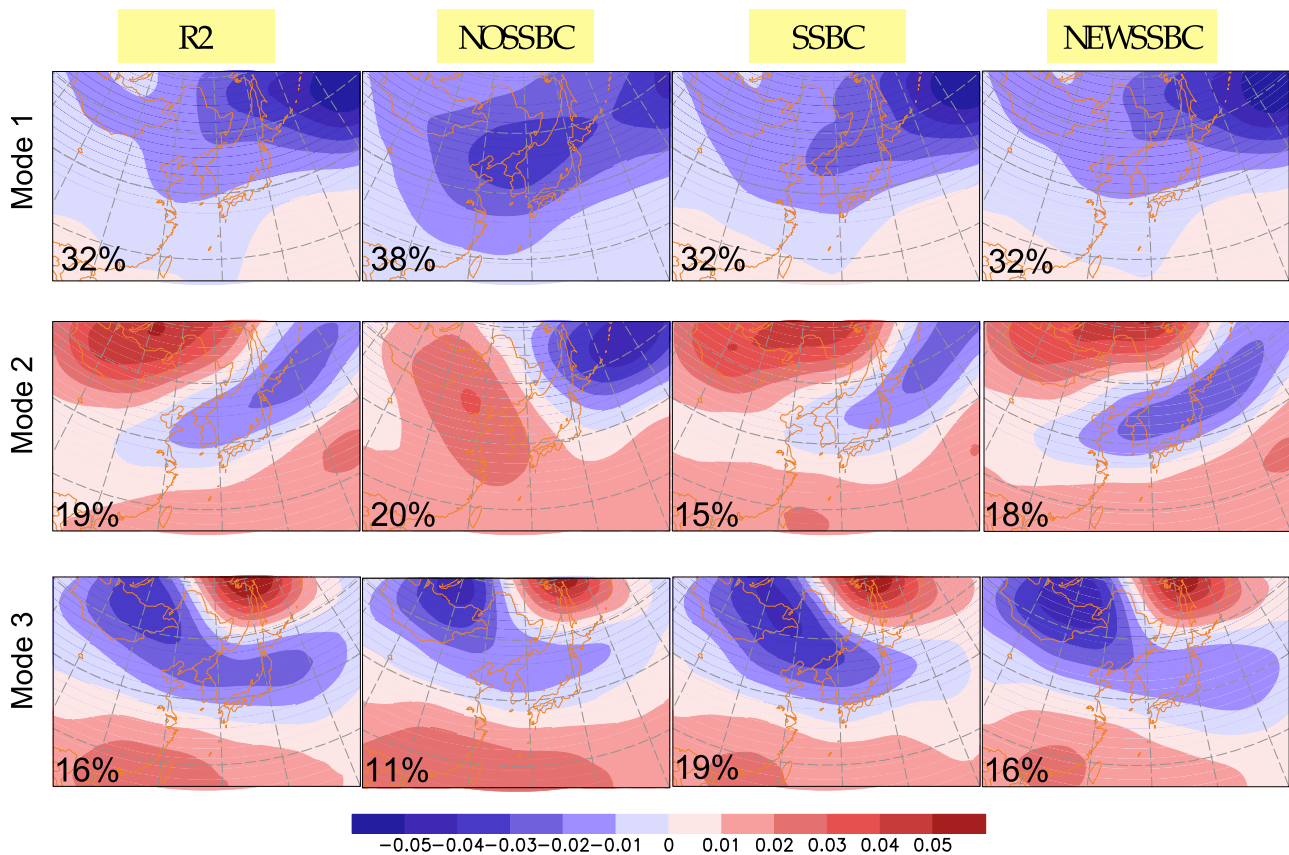
3.2. Empirical Orthogonal Function (EOF)

[18] The EOFs of summertime seasonal mean 500 hPa heights are compared in Figure 6 for the first three modes. The percentage variance explained by each mode is indicated in the figure. The first mode (top row) explains that more than 30% of the total variance in the NOSSBC (second column) has a pattern quite different from the others. Apparently, the regional model error adds error to the interannual variability and contaminates the low-frequency variability in global forcing. Mode 2 (second row) explains that about 20% of the total variance for the NOSSBC (second column) is also very different from that for R-2 and the others, while all the patterns look very similar for mode 3 (third row), which explains 15%–20% of the total variance. The SSBC corrections are working nicely as before. The original SSBC corrects most of the EOF errors, but the

interannual variability of 500-hPa height

Figure 5. Geographical distribution of interannual variability of seasonal mean 500 hPa height for summer (top row) and winter (bottom row). Units are meters. Note the different color coding for summer and winter.

Figure 6. Leading three modes of summertime 500 hPa geopotential height empirical orthogonal functions (EOFs) for analysis (R-2) and experiments during summer. Percentage variance is indicated in each plot.
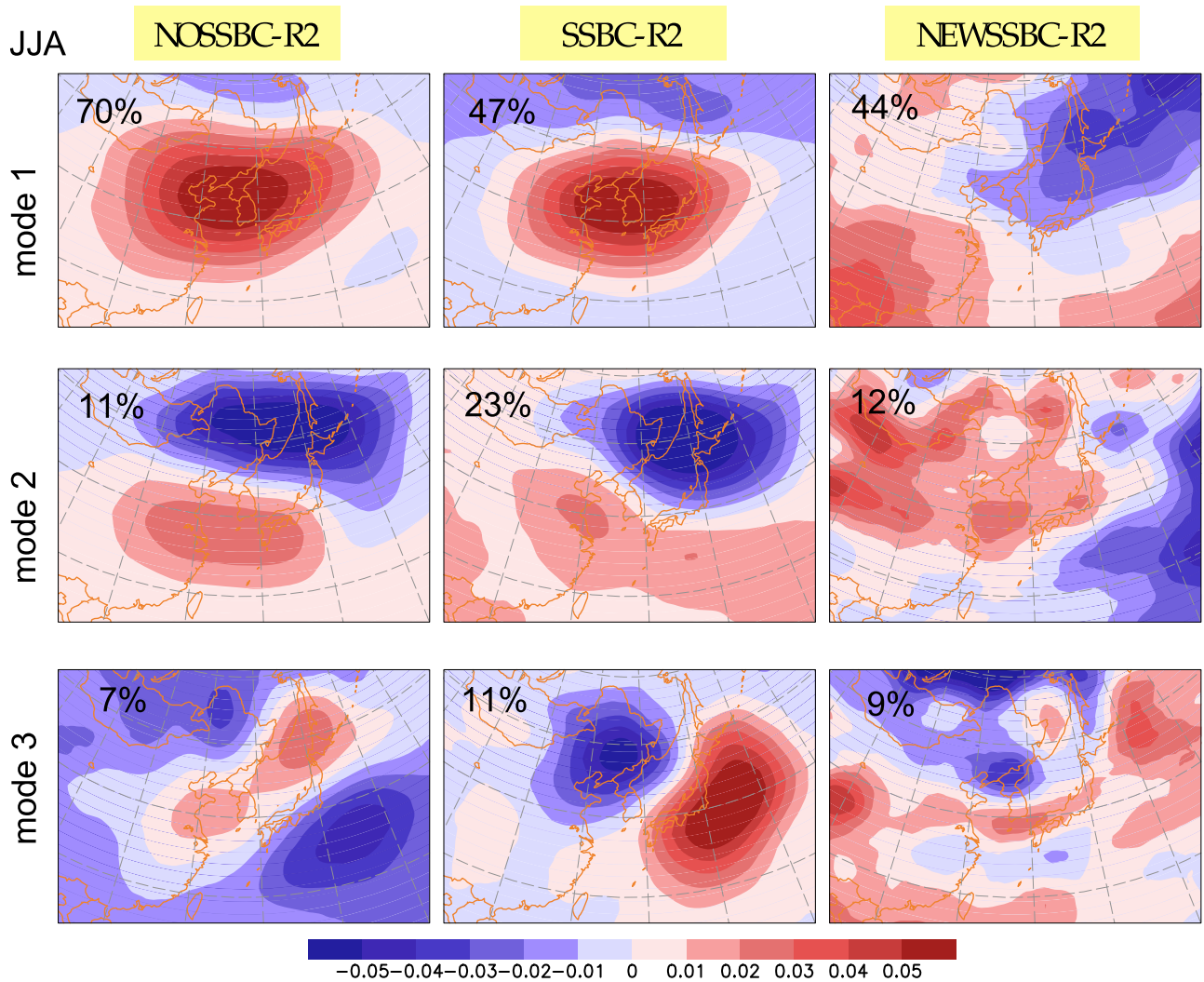
Figure 7. First three modes of EOFs of the 500 hPa height model error. Percentage variances are indicated in each plot.

refined SSBC produces EOF patterns much closer to those of R-2. The EOF of the difference between R-2 and each experiment is shown in Figure 7. There are distinct patterns in the NOSSBC and the original SSBC but not in the NEWSSBC. The model error tends to grow in an organized manner and varies from year to year in response to the change in external forcing. During winter, interannual variances are again different if the SSBC is not applied (Figure 5, second row). However, the first three modes of the EOF (Figure 8) are much more alike in all the experiments. This similarity is explained by the fact that the interannual variability in winter is generally larger than the variability of the model error. The temporal correlations between the time series of each EOF amplitude for observation (R-2) and simulations are reported in Table 1. The correlation improves significantly by applying the correction both in summer and in winter.
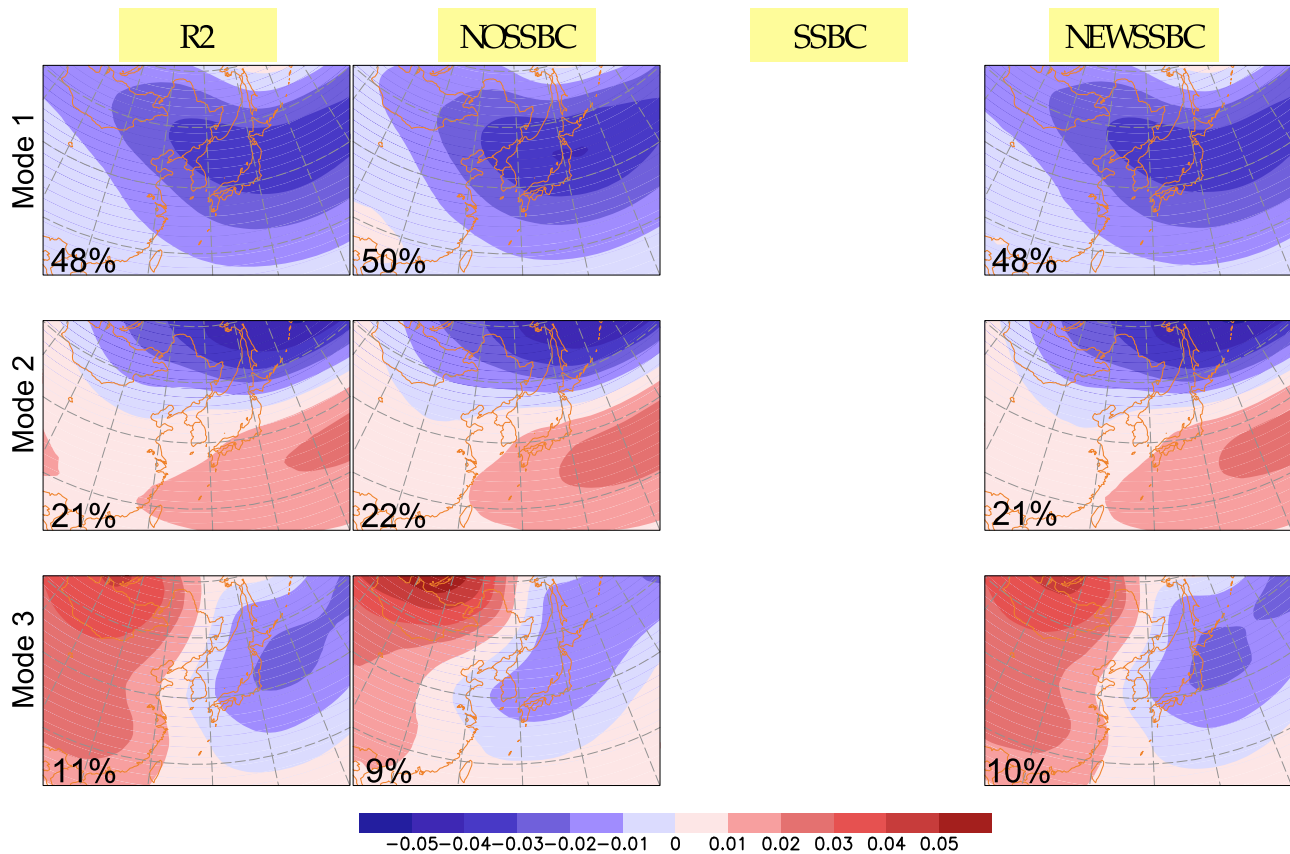
3.3. Linear Trend

[19] The linear trend of 500 hPa height is compared at each grid point by a least squares linear fit, and the slope is plotted in Figure 9. We see again that the NOSSBC is very different from R-2 in magnitude and pattern, and both corrections are working reasonably well. For example, the sign of the trend changes from negative in R-2 to positive in the NOSSBC over northern Japan in the summer. The pattern correlations between R-2 and the NOSSBC, SSBC, and NEWSSBC during summer are 0.68, 0.82, and 0.97, respectively. During the winter the pattern of the trend is fairly similar among the three experiments, but the magnitude is significantly underestimated in the NOSSBC run. The difference between R-2 and the NEWSSBC is greater than that in summer, and the NEWSSBC is worse than the SSBC in some places (e.g., the northeast corner) during winter, probably because of the large interannual variability during winter (Figure 5) and the sensitivity of the linear trend calculations from the rather short period of 25 years. The pattern correlations among R-2, the NOSSBC, and the NEWSSBC are the same, 0.96.

[20] In summary, the regional model has synoptic- to planetary-scale error that varies from year to year. This error contaminates the interannual variability. The magnitude of the error is large enough to modify the leading EOFs and even

Figure 8. Same as Figure 6 but during winter.

the sign of the linear trend in some locations, particularly in summer. The error correction scheme, if properly incorporated, can significantly reduce these errors.

4. Impact on Precipitation and Surface Temperature

[21] In the previous section the errors of interannual variabilities, namely, 500 hPa height, 850 hPa winds, and 200 hPa winds, were examined. Since these parameters are connected with the variables to which the SSBC is applied in the basic set of equations, it is not surprising that the SSBC reduces the error.

[22] The more important issues examined here are the errors in the derived fields, such as precipitation, near-surface temperature, surface and radiation fluxes, soil moisture, and many other parameters obtained during model integrations. In this section we examine precipitation and near-surface temperature, since these are the most frequently used variables for seasonal prediction, global change, and application studies. These variables may suffer from errors due to deficiencies in model physical parameterizations and insufficient resolution to resolve small-scale surface characteristics, even if the synoptic- to planetary-scale forcing is correct. As a result, we may not see the impact of the SSBC in those parameters as clearly as in the height and wind fields.

4.1. Mean Difference and Interannual Variance

[23] To start, let us examine the pattern of precipitation. Figure 10 compares precipitation between the observation

(CPC merged analysis of precipitation; CMAP [*Xie and Arkin*, 1997]) and the three experiments during summer and winter (two experiments for winter). In summer the model-produced precipitations are more similar to one another than to the observation, as shown by the widespread precipitation over the continent. The CMAP is a coarse-resolution precipitation analysis and we should not expect the small-scale features to agree with the model, but the difference in the synoptic- to planetary-scale pattern is clear. The small-scale precipitation over the main island of Japan, Korea, and coastal Russia is probably not obtainable from the CMAP. Among the downscaled analyses, SSBC has the largest overestimation, thus it stands out. This is a result of the area mean moisture correction, which has been removed in the NEWSSBC. The removal reduced the bias except over southern China, which was not in the NOSSBC to start
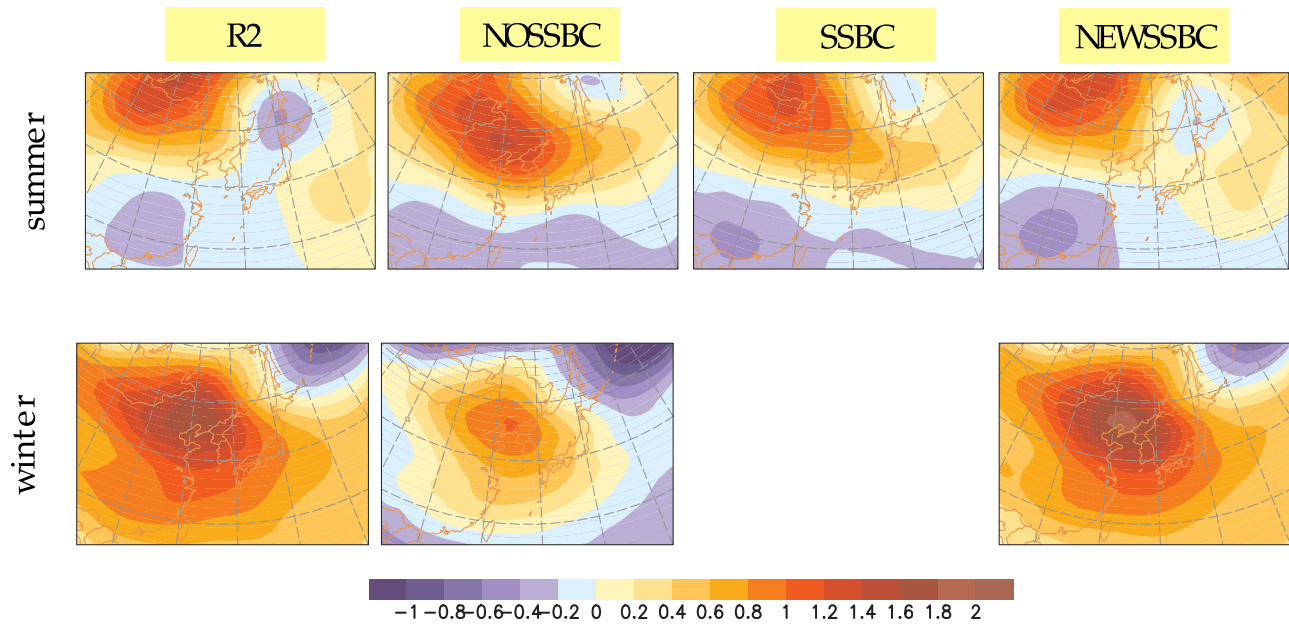
Table 1. Correlation of 500 hPa Height Empirical Orthogonal Function Time Series[a]

	NOSSBC	SSBC	NEWSSBC
Summer			
Mode 1	0.88	0.98	0.99
Mode 2	0.73	0.94	0.95
Mode 3	0.93	0.93	0.95
Winter			
Mode 1	0.84	—	0.99
Mode 2	0.81	—	0.93
Mode 3	0.52	—	0.88

[a]NEWSSBC, refined scale selective bias correction (SSBC); NOSSBC, SSBC without spectral nudging; SSBC, original SSBC.
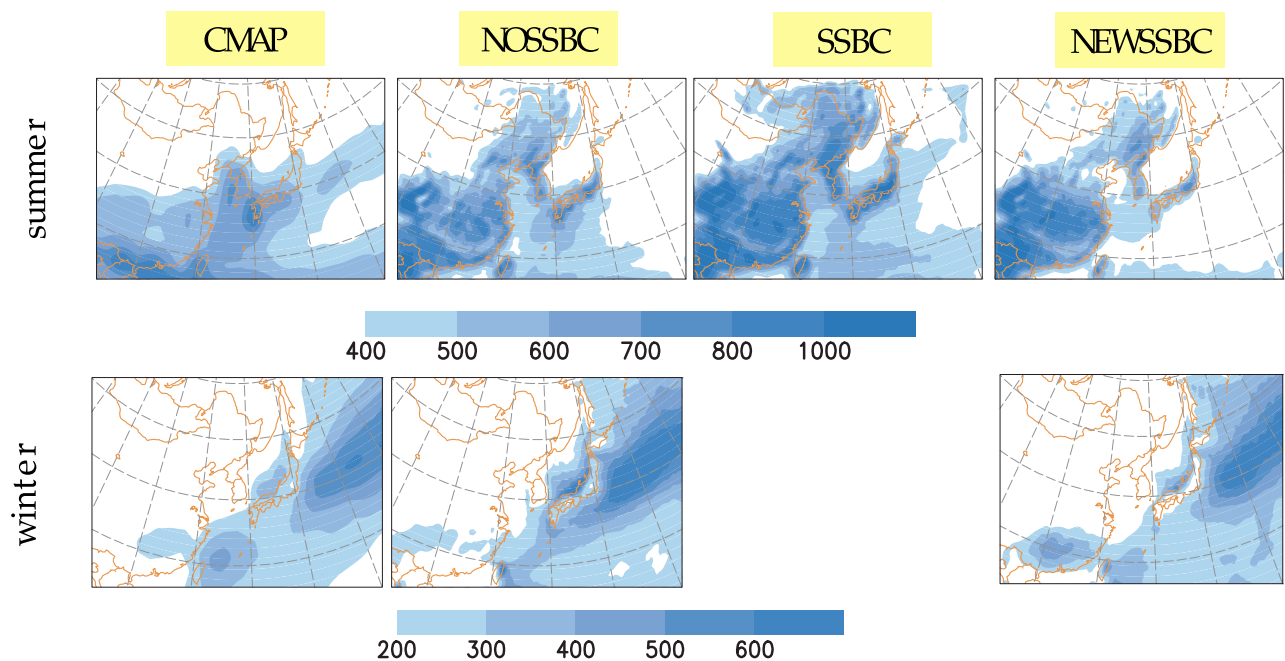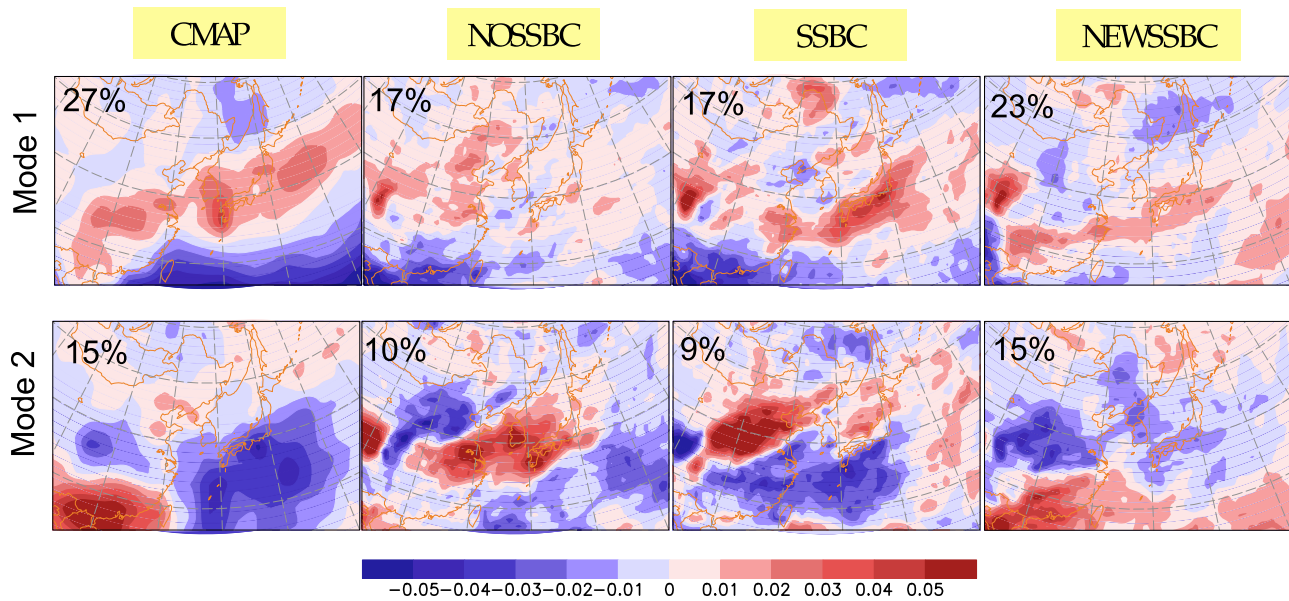
linear trend of 500-hPa height

Figure 9. The 1978–2003 linear trend at 500 hPa height for summer (top plots) and winter (bottom plots). Units are meters per 10 years.

Precipitation (mm)

Figure 10. The 1978–2003 climatology of precipitation for summer (top plots) and winter (bottom plots). Units are millimeters per month.

EOF of Precipitation (summer)

Figure 11. First two leading EOFs of seasonal mean precipitation during summer from observation (R-2) and experiments.

with. The correlation pattern of the synoptic- to planetary-scale precipitation pattern is computed by intentionally reducing the regional model resolution to that of the CMAP using the area average. The correlation declines from 0.64 to 0.49 and 0.46 for the NOSSBC, SSBC, and NEWSSBC, respectively, indicating much less impact on skill for the synoptic- to planetary-scale precipitation patterns. During the winter (Figure 10, second row) the model-produced synoptic- to planetary-scale precipitation patterns are very similar to one another and to observation (correlation of 0.91 for both experiments using the same spatial resolution with CMAP), with the exception of the small-scale precipitation maximum along Japan's Sea of Japan coastline, which cannot be resolved by the CMAP. The precipitation overestimation is apparent in the NOSSBC, but less so during the winter. These comparisons indicate that the synoptic- to planetary-scale precipitation pattern is not sensitively affected by the synoptic- to planetary-scale error in the atmospheric circulation, at least for this region and domain during winter. The discrepancy between the simulated precipitation and observation suggests that the model precipitation is more critically determined by parameterization, which is not properly responding to the synoptic- and planetary-scale forcing. The inability of the model physics to reproduce observed precipitation under observed forcing in single-column models has been well documented [*Hack and Pedretti*, 2000].

[24] With regard to the interannual variability we start observing significant differences among the model simulations. Figure 11 shows the EOF of precipitation during summer. Note that the variances explained by the two modes go only up to 40%. For mode 1 the model simulation patterns are not very similar to the observed pattern, but the NEWSSBC and SSBC resemble the CMAP more than the NOSSBC does. For example, the positive red band oriented

southwest to northeast is clearer in the SSBC and NEWSSBC. The large negative area near the southern boundary in the CMAP is not well reproduced by any of the models, but the weak negative area just west of Sakhalin is found in the NEWSSBC. The somewhat disorganized EOF patterns in the model simulations indicate that the model response to interannual variability is weaker in synoptic- to planetary-scale forcing, but the correction in synoptic- to planetary-scale atmospheric fields certainly helps to improve the simulation of precipitation variability. For the second mode all the model simulations differ greatly from the CMAP. During winter (Figure 12) the scenario is quite similar to that in summer, and the NEWSSBC is again slightly better in modes 1 and 2. There is a systematic difference in the location of the maxima in mode 1 for the NEWSSBC, which is shifted southward by 2°–3° latitude. The similarity between R-2 and the NEWSSBC in mode 2 is not strong, and the pattern is disorganized in NEWSSBC. Once again, the interannual variability of forcing is not directly reflected in the model simulation. Note that the EOFs of the NOSSBC agree much less than those of the NEWSSBC, indicating the modest impact of the SSBC on precipitation. The correlation of EOF time series with observation indicates a higher correlation for the NEWSSBC of up to 0.76 for mode 1 during winter, but it is generally much lower (table not shown).

4.2. Linear Trend

[25] Figure 13 compares the linear trend of precipitation during 1979–2005. The model simulations present much smaller scale patterns, with trends of opposite signs. However, synoptic- to planetary-scale patterns, such as the positive trend in southwest China, negative trend over the central-northern part of the domain, and positive trend over the northeast corner of the domain all agree with the CMAP

EOF Precipitation (winter)
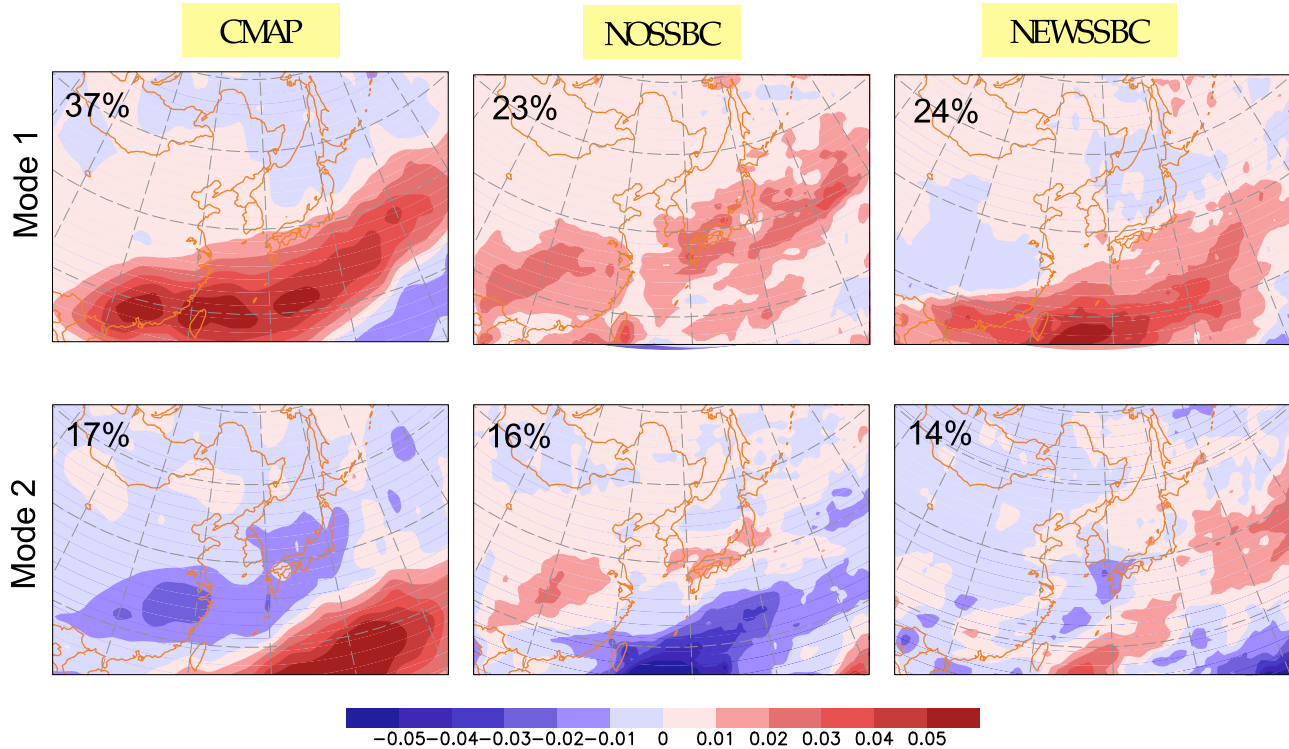
Figure 12. Same as Figure 11 but for winter.

trend in summer. The narrow band of negative trend oriented from northeast to southwest and located right over Japan in the NOSSBC seems to have a different orientation of east-northeast to west-southwest in the SSBC but is more disorganized in the NEWSSBC. The pattern correlations computed by matching the regional model resolution with that of the CMAP with area average are 0.21 for the NOSSBC, 0.26 for the SSBC, and 0.43 for the NEWSSBC, indicating decent improvements by the NEWSSBC. During winter, even the synoptic- to planetary-scale patterns are not very similar, with a much enhanced trend in the model simulations. Pattern correlations for the NOSSBC and NEWSSBC are 0.02 and −0.06, respectively. Apparently, the linear trend of precipitation is very sensitive to the small change in the synoptic- to planetary-scale forcing field.

[26] Figure 14 compares the linear trend of near-surface air temperature. It should be noted that over ocean, the trend is mostly controlled by the SST analysis and thus it is nearly the same for the NOSSBC, SSBC, and NEWSSBC experiments and is not affected by the synoptic- to planetary-scale correction. In summer all the model simulations agree well with R-2, while in winter the NEWSSBC seems to agree better with the observed trend, particularly the larger extent of the positive trend over China. The pattern correlations during summer for the NOSSBC, SSBC, and NEWSSBC are 0.89, 0.86, and 0.86, respectively, while in winter they are 0.4 for the NOSSBC and 0.6 for the NEWSSBC. The near-surface temperature trend seems to be less sensitive to the change in synoptic- to planetary-scale forcing during summer but is more sensitive in winter. This may be ex-

plained by the fact that the near-surface temperature is more strongly controlled by land surface conditions (soil moisture and surface albedo) in summer, while in winter it is influenced more strongly by synoptic- to planetary-scale circulation. Therefore, the impact of the SSBC can be more apparent during the winter season.

4.3. Validation of Precipitation Against Station Observations

[27] Since the CMAP represents coarse-resolution synoptic- to planetary-scale features of the observed precipitation, it may not be appropriate for the validation of simulated small-scale model precipitation. We compared simulated precipitations directly with station observations over Japan, where mesoscale hourly precipitation observations are readily available. The observation Automatic Meteorological Data Acquisition System (AMeDAS) network [*Takase et al.*, 1988] is distributed throughout Japan, with the average station distance being 20–30 km. Figure 15 compares summer- and wintertime seasonal correlations of seasonal mean precipitation against 3 hourly AMeDAS observations averaged over several subregions over Japan (Figure 15a). During June-July-August (Figure 15b) the correlation is about 0.6–0.8 for all areas with the NEWSSBC, which is much better than the other experiments and clearly demonstrates the effectiveness of the SSBC in simulating the interannual variability of the seasonal mean precipitation. The improvement is not as large during winter (Figure 15c), but some northern areas (North Hokkaido and South Hokkaido) show better agreement. This validation against observation
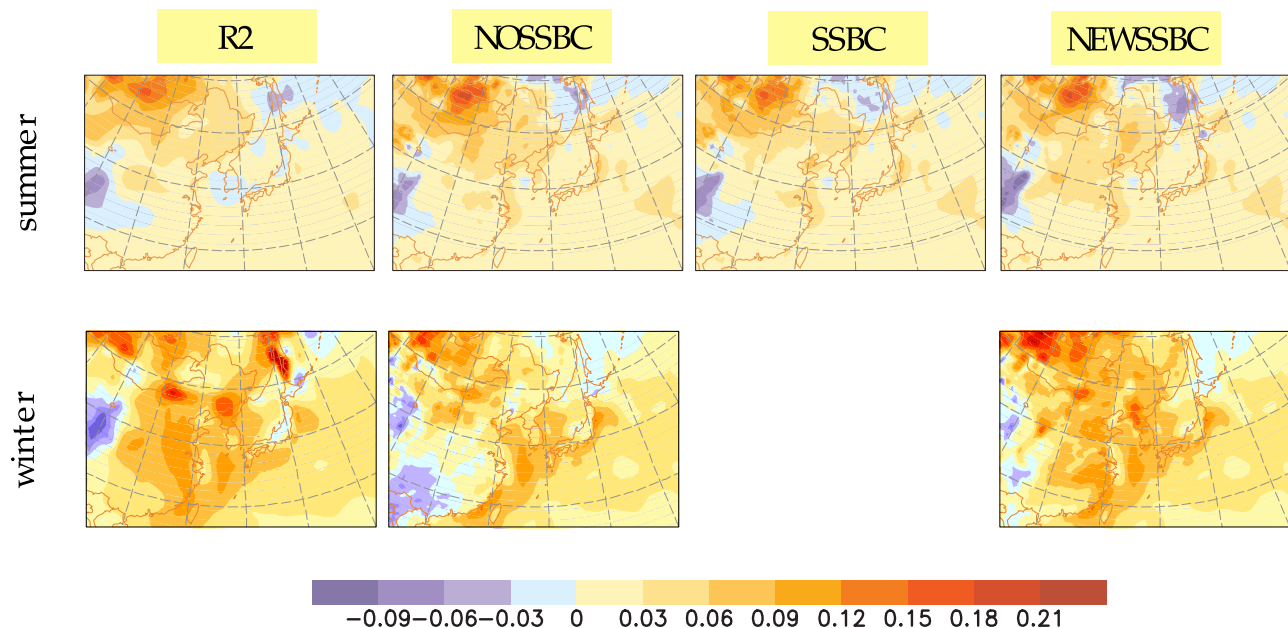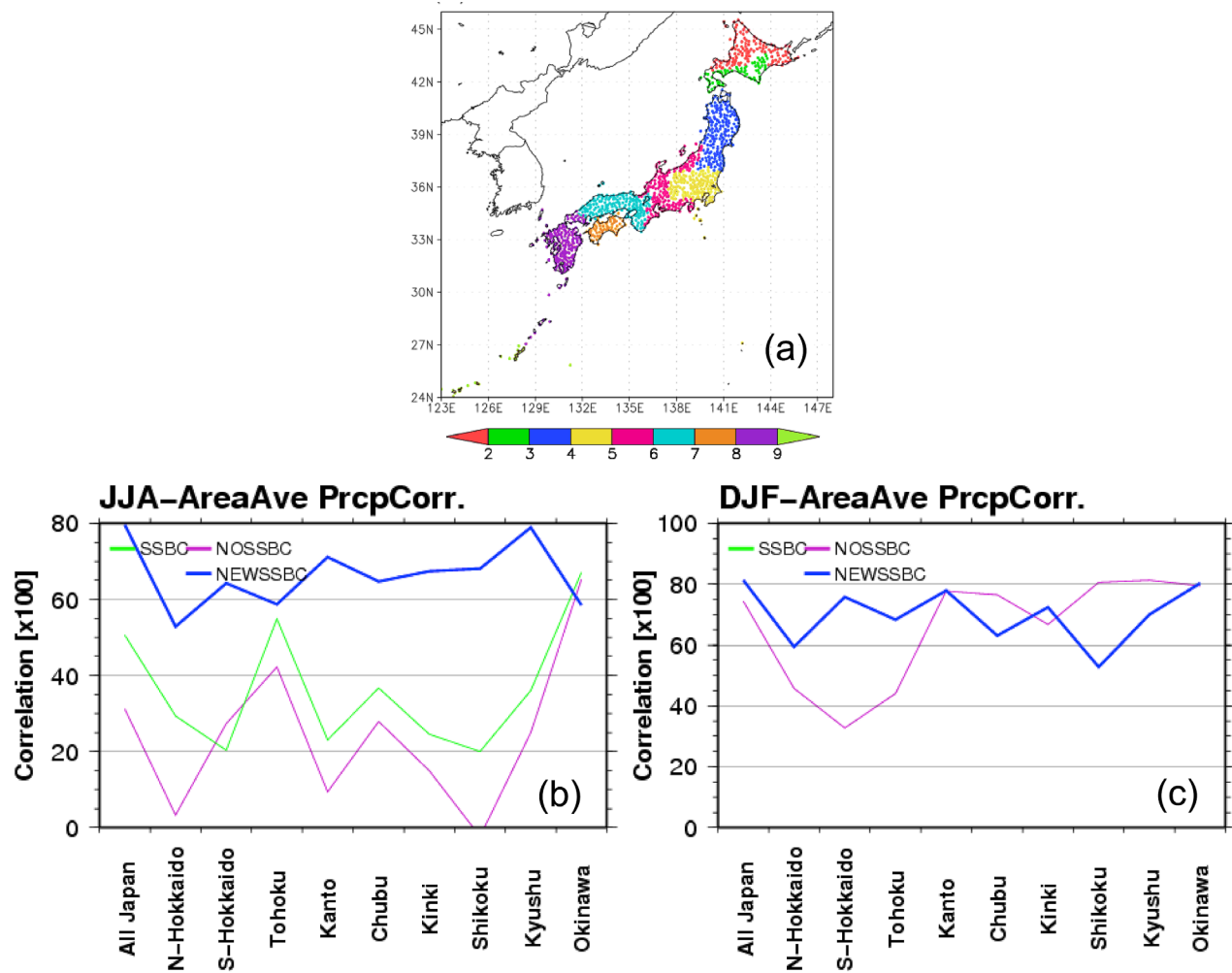
Linear trend of precipitation
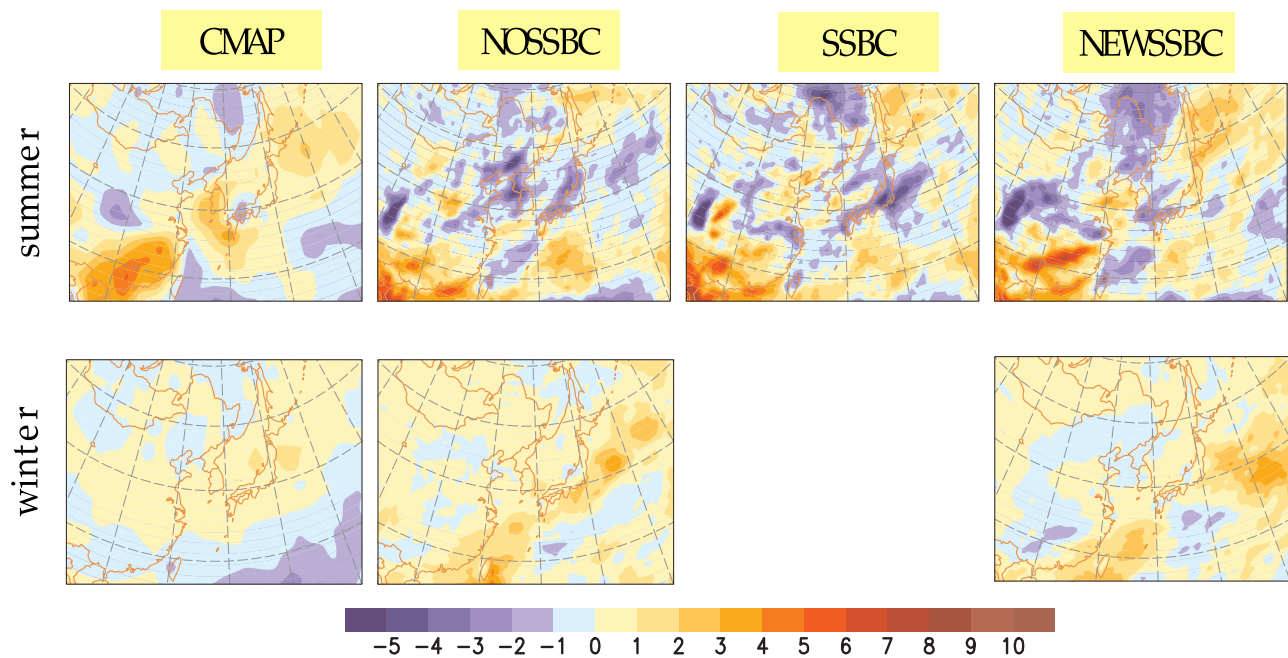
Figure 13. The 1978–2003 linear trend of precipitation during summer (top plots) and winter (bottom plots). Units are millimeters per 10 years.

Linear trend of surface temperature

Figure 14. The 1978–2003 linear trend of near-surface temperature during summer (top plots) and winter (bottom plots). Units are millimeters per 10 years.

Figure 15. Temporal correlation of precipitation at Automatic Meteorological Data Acquisition System (AMeDAS) stations averaged over subdomains in (b) summer and (c) winter. (a) Domains are color coded by orange (North Hokkaido), green (South Hokkaido), magenta (Tohoku), yellow (Kantou), red (Chubu), blue (Kinki), brown (Shikoku), purple (Kyushu), and light green (Okinawa).

again suggests that the correction to synoptic- to planetary-scale forcing is important in properly simulating the interannual variability of precipitation on the mesoscale.

5. Relation to the Error in Day-to-Day Variability and Possible Causes of the Error in Interannual Variability

[28] The errors of the regional simulation can be classified into the following three groups, depending on their characteristic time scales.

[29] 1. The first is the systematic error in the conventional sense, which is defined as a long-term multiyear mean difference between observed and simulated fields. This error may be alternatively called the long-term mean error.

[30] 2. The second is the seasonal (or monthly) mean difference between observed and simulated fields for a particular year, which varies from year to year. This class may be called the low-frequency error.

[31] 3. The third is the day-to-day difference between observed and simulated fields, which varies daily. This class

may be called the high-frequency error. There are other classes of errors with much higher (diurnal) and lower (multidecadal) frequencies, but we do not deal with them in this paper.

[32] In this study we have examined the first two classes of errors and demonstrated that they are of appreciable amplitude (long-term mean error in Figures 1–3 and other errors in Figures 4–15). This paper's unique contribution is that the low-frequency error is of significant amplitude and may lead to false results if the year-to-year variabilities of downscaled products without spectral nudging are used.

[33] Since the long-term mean, low-frequency, and high-frequency modes interact with each other in reality, it may be useful to examine the "systematic error" in the high-frequency mode activity. This has been studied by *Rockel et al.* [2008], in which systematic loss of kinetic energy has been noted for the two grid-point models they tested (Climate version of the Local Model of the German Weather Service [*Steppeler et al.*, 2003] and Regional Atmospheric Modeling System [*Pielke et al.*, 1992]). These high-frequency mode errors may cause systematic error of

day-to-day variance of 500-height
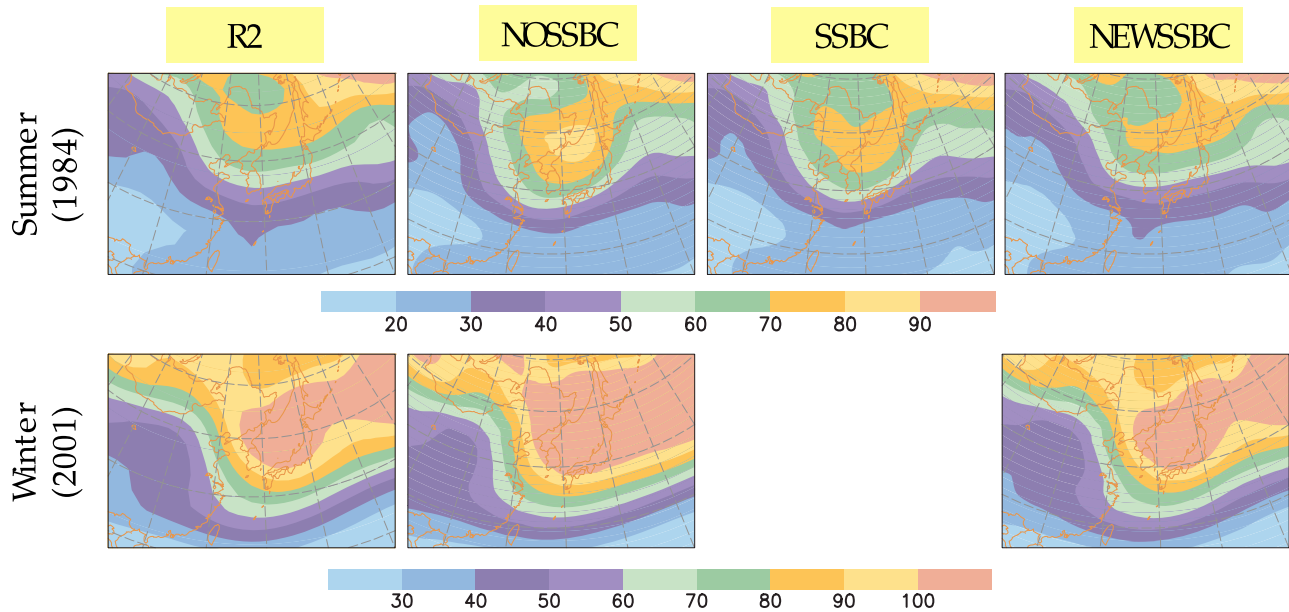
Figure 16. Daily variance at 500 hPa height for R-2 and experiments. Top row is for summer 1984 and bottom row is for winter 2001. These 2 years were selected as the amplitudes of the low-frequency errors are high. Note the increase in daily variance for summer and winter for the NOSSBC compared to R-2.

the low-frequency mode through scale interactions. They did not mention this possibility because of the relatively short integration period (15 days) in their experiment. We examined the day-to-day variability in our simulation to determine the possible cause of the low-frequency mode error. In Figure 16 we compare day-to-day variability of the 500 hPa height between R-2 and three experiments. We chose the year when the systematic error in the low-frequency mode is largest for each season. Figure 16 indicates that the day-to-day variability is slightly increased in the NOSSBC run, which is in contrast with the results of Rockel *et al.* We suspect that this behavior is due to the spectral method used in the RSM, which does not have the dissipating effect of finite differencing.

[34] Because of the small systematic error in high-frequency variability in the RSM, the error in the low-frequency mode may be considered a result of some sort of forced response. Looking at the EOF of error in Figure 7 (NOSSBC-R2), the patterns for modes 1 and 2 seem to suggest the formation of stationary waves. These patterns are probably excited by the lateral forcing and maintain their amplitude via the ill-conditioned lateral boundary treatment and the inconsistencies between the global and the regional solutions. The amplitude of the low-frequency error is governed by the external forcing, which varies from year to year, resulting in the low-frequency error.

6. Conclusions

[35] This paper examines the role of synoptic- to planetary-scale error in regional models and its effect on interannual

variability in dynamical downscaling. For this purpose, dynamical downscaling of the NCEP/DOE reanalysis during 1979–2003 over far eastern Asia, using the Scripps Institution of Oceanography Regional Spectral Model at 50 km resolution, is performed. The model was run during summer (June-July-August) and winter (December-January-February) for 25 years.

[36] It has been demonstrated that a synoptic- to planetary-scale error correction must be applied to the conventional dynamical downscaling method or it will suffer from regional model error of the same scale, which contaminates the interannual variability and linear trend of the downscaled fields. This will apply to most regional models, since the skill of the RSM is very compatible with that of other models [e.g., *Takle et al.*, 1999; http://narccap.ucar.edu/results/ncep-results.html]. The error also contaminates the low-frequency variability and trend of derived fields, such as precipitation. The effect of model error on the variability is greater in summertime, as the magnitude of the error is comparable to the interannual variability of seasonal mean.

[37] The sources of the low-frequency mode error can be complex. The systematic error in the day-to-day variability was computed to determine the possible source of the error, but the model showed very few problems. From the EOF patterns of the 500 hPa error, it is speculated that the low-frequency error is a reflection of the stationary computational mode excited by inconsistencies in the regional and external solutions amplified by the ill-posed lateral boundary condition.

[38] To improve the downscaling the original version of the SSBC [*Kanamaru and Kanamitsu*, 2006] was refined to

further reduce the synoptic- to planetary-scale model error. This was accomplished by replacing the tendency nudging in the original version with the field nudging itself, nudging the rotational part of the wind only, removing the area average moisture correction, and reducing the lateral boundary nudging zone width and strength. The refined SSBC reduced the error of the interannual variability of seasonal mean 500 hPa height to within 5 m, nearly eliminating it.

[39] The impact of correcting the synoptic- to planetary-scale error in simulating precipitation and near-surface temperature was modest. This somewhat diminished impact is due to inaccuracies in the model's precipitation process, which cannot faithfully reproduce the observed precipitation, particularly its interannual variability, even when the synoptic- to planetary-scale forcing is specified. However, the modest impact implies that even with somewhat deficient parameterization, the correction to the synoptic- to planetary-scale forcing works positively to reduce error and improve dynamical downscaling. In this context the application of a correction scheme that effectively reduces the synoptic- to planetary-scale error is very important.

[40] The question that needs to be answered next is whether spectral nudging should be applied to the downscaling of seasonal forecast and global change simulations, for which no observation is available but the large-scale features are unquestionably contaminated by model errors. Answering this question requires discussion of the following somewhat controversial issues: (1) Can regional models make better forecasts or simulations of synoptic- to planetary-scale features? and (2) How should the chaotic nature of the atmosphere and model be treated? The first question is connected to how much the synoptic- to planetary-scale motion in the regional domain is trusted, and the second question is how to deal with the situation where no single truth exists. We will hopefully answer these questions in the future, as a continuation of this work.

Appendix

[41] This Appendix briefly reviews the original SSBC scheme, introduces the refined methods, and outlines their performance. The original scheme described in KK06 is based on ideas proposed by *Kida et al.* [1991] and *von Storch et al.* [2000]. In the original scheme a term is introduced to the zonal and meridional momentum equations to "nudge" the difference between the background global model and analysis field and the regional forecast field (hereafter called perturbation) to 0 for a scale greater than a critical length in two-dimensional wave space.

$$F_t^{\text{new}}(m,n) - F_{t-\Delta}(m,n) = \left(\frac{1}{1+\alpha}\right)\left(F_t^{\text{old}}(m,n) - F_{t-\Delta}(m,n)\right)$$

$$\text{for} \quad m,n, < m_c, n_c, \tag{A1}$$

where F_t is the perturbation, expressed in spectral coefficient form, with two-dimensional wave numbers m and n (in the x and y directions, respectively) at time t. $F_{t-\Delta}$ is a spectral coefficient one time step earlier. The superscripts "old" and "new" indicate the values before and after the damping. A damping coefficient α has a value of 0.9, which is deter-

mined from multiple trial-and-error integrations and is constant with height, which differs from other spectral nudging methods. KK06 noted that the simulation is not very sensitive to the choice of this coefficient. (Equation A1) is derived from an implicit time scheme to avoid numerical instability. Note that in this formulation, the damping is applied to the time tendency of the perturbations. The critical scale is set to the physical scale of 1000 km, and consequently, the critical wave numbers m_c and n_c vary with domain size and model resolution. For temperature and moisture the area average perturbation is set to 0 every time step, but no damping is applied to the wave coefficients. In addition, the surface pressure is corrected to account for the difference in surface altitude between the coarse-resolution global model and analysis and the regional model. Using these methods, KK06 demonstrated that the synoptic- to planetary-scale fields do not deviate significantly from global forcing, the simulation becomes insensitive to the choice of domain size, and the precipitation simulation skill improves.

[43] During the validation of long-term downscaling of reanalysis (CaRD10 [*Kanamaru and Kanamitsu*, 2007; *Kanamitsu and Kanamaru*, 2007]), the synoptic- to planetary-scale error within the domain can occasionally grow to a significant amplitude even with the SSBC. We performed further experiments to improve the SSBC by more carefully selecting the nudging variables, nudging method, and magnitude of nudging. We also discovered that the lateral boundary nudging zone width and strength are closely related to the amplitude of the synoptic- to planetary-scale model error, which is controlled by the SSBC. The lateral boundary zones used in the original SSBC are rather broad, 23% of the zonal and meridional lengths of the domain (11.5% for each side), which reduces the usable domain region by nearly 40%. Even a small reduction of the nudging zone is beneficial to allow for a wider regional domain.

[44] After many trial runs we found that the following five modifications decreased the errors, improved the model performance, and reduced the lateral boundary zone.

[45] 1. The nudging is applied to perturbation rather than its tendency with the same nudging coefficient. This constrains the error and keeps it small.

$$F_t^{\text{new}}(m,n) = \left(\frac{1}{1+\alpha}\right)F_t^{\text{old}}(m,n) \quad \text{for} \quad m,n < m_c, n_c. \tag{A2}$$

[46] 2. The nudging is applied only to the rotational part of wind. This minimizes spurious surface pressure oscillations and tends to better maintain the synoptic- to planetary-scale balance between mass and motion fields.

[47] 3. The area-averaged correction of moisture is removed, and only the area-averaged temperature is corrected. The removal of the moisture correction minimizes the significant bias in the precipitation simulation caused by inconsistencies between the physical packages of the forcing and the regional model, especially at lower latitudes.

[48] 4. By applying stronger spectral nudging over the domain combined with all the other modifications, it became possible to narrow the lateral boundary zones to 5% (from the original 23%) of the zonal and meridional width of the domain (2.5% on each side) and reduce the nudging coefficients to a minimum to keep the integrations stable.

Table A1. Performance of Regional Model Integrations with Different Spectral Nudging Methods and Boundary Condition Treatments[a]

	500 hPa Height RMS (m)	Sea Level Pressure RMS (Pa)	Total Precipitation (mm/day)
North America			
NOSSBC	21.1	300.8	1.59
SSBC	23.3	264.0	1.99
NEWSSBC	13.8	214.0	1.52
Tropical South America			
NOSSBC	28.7	377.7	4.51
SSBC	11.4	158.0	8.30
NEWSSBC	11.3	151.8	4.67

[a]NEWSSBC, refined scale selective bias correction (SSBC); NOSSBC, SSBC without spectral nudging; RMS, root-mean-square; SSBC, original SSBC.

[49] 5. Diabatic processes are removed from the lateral boundary zone, although the impact is minimal.

[50] We do not discuss the new SSBC method in further detail since we are still not fully satisfied with its application. There are too many empirical parameters determined by a large number of experiments, which are still not optimal. We are in the process of developing a new method based on the objective analysis technique, in which the weighted sum of the initial guess (forecast) and the observation is used to obtain the most likely analysis. We may be able to apply this method for different spatial scales based on the accuracy of the regional forecast.

[51] We performed three experiments: (1) the original SSBC; (2) a narrow lateral boundary zone without the SSBC (NOSSBC); and (3) a new, improved SSBC (NEWSSBC) with a narrow lateral boundary zone. To examine the more general performance of the refined SSBC, the integrations were performed over two regions: one over the North American domain (10–50°N, 65–135°W) and the other over the Tropical South American domain (20°S–15°N, 30–90°W). The integration period was arbitrarily chosen from 1 to 10 March 1985. The RMS differences from the forcing fields, NCEP/DOE R-2, are used as a measure of the synoptic- to planetary-scale error. We exclude details of the model descriptions used in this study, except that they are very similar to those described in section 3.1.

[52] Table A1 summarizes the results of these experiments. The refined SSBC worked best over both North America and South America in reducing 500 hPa height RMS error, although the improvement was less marked in the tropics. The improvement in surface pressure is also apparent. The SSBC generally improves the fit of the mass field (except for the small degradation of 500 hPa height in North America). The overestimation of precipitation in the original SSBC was corrected in both the NOSSBC and the refined SSBC by removal of the area-averaged correction of moisture. These experiments suggest that the refined SSBC considerably improves on the original SSBC. This method has been successfully applied to a separate study that deals with the specification of the lateral boundary problem [Yoshimura and Kanamitsu, 2009] and the downscaling of global change simulations (study in progress).

References

Blackmon, L. M. (1976), A climatological spectral study of the 500 mb geopotential height of the Northern Hemisphere, *J. Atmos. Sci.*, *33*, 1607–1623.

Davies, H. C. (1976), A lateral boundary formulation for multi-level prediction models, *Q. J. R. Meteorol. Soc.*, *102*, 405–418.

Davies, H. C. (1983), Limitations of some common lateral boundary schemes used in regional NWP models, *Mon. Weather Rev.*, *111*, 1002–1012.

Gochis, D. J., W. J. Shuttleworth, and Z.-L. Yang (2002), Sensitivity of the modeled North American monsoon regional climate to convective parameterization, *Mon. Weather Rev.*, *130*, 1282–1297.

Hack, J. J., and J. A. Pedretti (2000), Assessment of solution uncertainties in single-column modeling frameworks, *J. Climate*, *13*, 352–365, doi:10.1175/1520-0442(2000)013<0352:AOSUIS>2.0.CO;2.

Hong, S.-Y., and H.-M. H. Juang (1998), Orography blending in the lateral boundary of a regional model, *Mon. Weather Rev.*, *126*, 1714–1718.

Hong, S.-Y., and A. Leetmaa (1999), An evaluation of the NCEP RSM for regional climate modeling, *J. Climate*, *12*, 592–609.

Hong, S.-Y., Y. Noh, and J. Dudhia (2006), A new vertical diffusion package with an explicit treatment of entrainment processes, *Mon. Weather Rev.*, *134*, 2318–2341.

IPCC (2007) Climate change 2007: The physical science basis, in *Contribution of the Working Group I to the Fourth Assessment Report of the Intergovernmental Panel on Climate Change*, edited by S. Solomon, D. Qin, M. Manning, Z. Chen, M. Marquis, K. B. Averyt, M. Tignor, and H. L. Miller, Cambridge University Press, Cambridge.

Juang, H.-M. H., and M. Kanamitsu (1994), The NMC nested regional spectral model, *Mon. Weather Rev.*, *122*, 3–26.

Juang, H.-M. H., S.-Y. Hong, and M. Kanamitsu (1997), The NCEP regional spectral model: An update, *Bull. Am. Meteorol. Soc.*, *78*, 2125–2143.

Kanamaru, H., and M. Kanamitsu (2006), Scale selective bias correction in a downscaling of global analysis using a regional model, *Mon. Weather Rev.*, *135*, 334–350, doi:10.1175/MWR3294.1.

Kanamaru, H., and M. Kanamitsu (2007), 57-year California reanalysis downscaling at 10 km (CaRD10): Part II. Comparison with North American regional reanalysis, *J. Climate*, *20*, 5553–5571, doi:10.1175/2007JCLI1522.1.

Kanamitsu, M., and H. Kanamaru (2007), 57-year California reanalysis downscaling at 10 km (CaRD10): Part I. System detail and validation with observations, *J. Climate*, *20*, 5527–5552, doi:10.1175/2007JCLI1482.1.

Kanamitsu, M., W. Ebisuzaki, J. Woollen, S.-K. Yang, J. J. Hnilo, M. Fiorino, and G. L. Potter (2002), NCEP-DOE AMIP-II reanalysis (R-2), *Bull. Am. Meteorol. Soc.*, *83*, 1631–1643.

Kang, H.-S., and S.-Y. Hong (2008), Sensitivity of the simulated East Asian summer monsoon climatology to four convective parameterization schemes, *J. Geophys. Res.*, *113*, D15119, doi:10.1029/2007JD009692.

Kida, H., T. Koide, H. Sasaki, and M. Chiba (1991), A new approach for coupling a limited area model to a GCM for regional climate simulations, *J. Meteorol. Soc. Jpn.*, *69*, 723–728.

Kusunoki, S., J. Yoshimura, H. Yoshimura, A. Noda, K. Oouchi and R. Mizuta (2006), Change in Baiu rain band in global warming projection by an atmospheric general circulation model with a 20-km grid size, *J. Meteorol. Soc. Jpn.*, *84*, 581–611.

Mahrt, L., and H.-L. Pan (1984), A two layer model of soil hydrology, *Boundary Layer Meteorol.*, *29*, 1–20.

Pielke, R. A., Sr., et al. (1992), A comprehensive meteorological modeling system—RAMS, *Meteorol. Atmos. Phys.*, *49*, 69–91.

Reynolds, R. W., and T. M. Smith (1994), Improved global sea surface temperature analyses using optimum interpolation, *J. Climate*, *7*, 929–948.

Rockel, B., C. L. Castro, R. A. Pielke Sr., H. von Storch, and G. Leoncini (2008), Dynamical downscaling: Assessment of model system dependent

retained and added variability for two different regional climate models, *J. Geophys. Res.*, *113*, D21107, doi:10.1029/2007JD009461.

Steppeler, J., G. Doms, U. Schattler, H.-W. Bitzer, A. Gassmann, U. Damrath and G. Gregoric, (2003), Meso-gamma scale forecast using the nonhydrostatic model LM, *Meteorol. Atmos. Phys.*, *82*, 75–96.

Takase, K., et al. (1988), Operational precipitation observation system in the Japan Meteorological Agency, in *Tropical Rainfall Measurements*, edited by J. S. Theon and N. Fugono, pp. 407–413, A. Deepak, Hampton, Va.

Takle, E. S., et al. (1999), Project to Intercompare Regional Climate Simulations (PIRCS): Description and initial results, *J. Geophys. Res.*, *104*, 19443–19462.

von Storch, H., H. Langenberg, and F. Feser (2000), A spectral nudging technique for dynamical downscaling purposes, *Mon. Weather Rev.*, *128*, 3664–3673.

Xie, P., and P. Arkin (1997), Global precipitation: A 17-year monthly analysis based on gauge observations, satellite estimates, and numerical model outputs, *Bull. Am. Meteorol. Soc.*, *78*, 2539–2558.

Yoshimura, K., and M. Kanamitsu (2009), Specification of external forcing for regional model integrations, *Mon. Weather Rev.*, *137*, 1409–1421.

S.-Y. Hong and Y.-B. Yhang, Department of Atmospheric Sciences and Global Environment Laboratory, Yonsei University, 134 Shinchon-dong, Seodaemun-ku, Seoul 120-749, Korea.

M. Kanamitsu and K. Yoshimura, Scripps Institution of Oceanography, University of California, 8605 La Jolla Shores Dr., La Jolla, CA 92093-0224, USA. (mkanamitsu@ucsd.edu)